

Photoluminescence Enhancement for Efficient Mixed-Halide Blue Perovskite Light-Emitting Diodes

Zhan Chen, Xiao-Ke Liu,* Heyong Wang, Xianjie Liu, Lintao Hou,* and Feng Gao

The development of highly efficient blue perovskite light-emitting diodes (PeLEDs) remains a big challenge, requiring more fundamental investigations. In this work, significant photoluminescence enhancement in mixed halide blue perovskite films is demonstrated by using a molecule, benzylphosphonic acid, which eventually doubles the external quantum efficiency to 6.3% in sky-blue PeLEDs. The photoluminescence enhancement is achieved by forming an oxide-bonded perovskite surface at grain boundaries and suppressing electron–phonon interaction, which enhances the radiative recombination rate and reduces the nonradiative recombination rate, respectively. Moreover, severe thermal quenching is observed in the blue perovskite films, which can be explained by a two-step mechanism involving exciton dissociation and electron–phonon interaction. The results suggest that enhancing the radiative recombination rate and reducing the electron–phonon interaction-induced nonradiative recombination rate are crucial for achieving blue perovskite films with strong emission at or above room temperature.

optical properties of metal halide perovskites, such as excellent color purity, readily tunable emission color, and solution process capability.^[1] Significant breakthroughs have been made in promoting the efficiency of PeLEDs.^[1] While green, red, and near-infrared PeLEDs have reached external quantum efficiencies (EQEs) over 20%,^[2–5] the EQEs of blue PeLEDs remain moderate.^[6–15] Since blue light is essential in the practical applications of lighting and displays, realizing high-efficiency blue PeLEDs is important and urgent.

Blue-emitting perovskite films with high photoluminescence quantum yields (PLQYs) are the key to highly efficient blue PeLEDs. The EQE of PeLEDs can be expressed by

$$\text{EQE} = \varnothing_{\text{PL}} \times \gamma \times \eta_{\text{oc}} \quad (1)$$

1. Introduction


Over the past several years, perovskite light-emitting diodes (PeLEDs) have attracted great attention owing to the appealing

where \varnothing_{PL} is the PLQY of the emissive layer, γ is the balance factor of charge–carrier injection, and η_{oc} is the light outcoupling efficiency.^[16,17] For PeLEDs with common planar device architectures, where η_{oc} is assumed to be a constant and balanced charge–carrier injection is achievable through device optimization, Equation (1) indicates that the PLQY of the emissive layer is a key determining factor of EQE.

For blue PeLEDs based on mixed chloride/bromide (Cl/Br) perovskites, a critical issue is that the PLQYs of mixed Cl/Br perovskite emissive layers deteriorate with increasing Cl/Br ratio. Mixed Cl/Br perovskites are a convenient way to make blue PeLEDs because their emission wavelengths can be readily tuned from greenish blue to deep blue by increasing Cl/Br ratio.^[6,18,19] However, increasing the Cl/Br ratio of mixed Cl/Br perovskite films usually decreases their PLQYs.^[20–22] This problem hinders the development of high-efficiency blue, especially deep blue, PeLEDs. Some reports demonstrated enhanced PLQYs in mixed Cl/Br perovskite films by reducing trap-assisted nonradiative recombination, for instance through defect passivation or crystallization control.^[6,9,23–29] Albeit these breakthroughs, rare attention has been given to other limiting factors of PLQY in mixed Cl/Br perovskite films.

Herein, we report significantly enhanced PLQY in mixed Cl/Br perovskite films by incorporating benzylphosphonic acid (denoted as BPA, see chemical structure in **Figure 1a**) as an additive. We find that BPA considerably promotes the radiative recombination rate in the mixed Cl/Br perovskite film by forming an oxide-bonded perovskite surface at grain

Z. Chen, L. Hou
 Guangzhou Key Laboratory of Vacuum Coating
 Technologies and New Energy Materials
 Siyuan Laboratory
 Department of Physics
 Jinan University
 Guangzhou 510632, P. R. China
 E-mail: thlt@jnu.edu.cn
 Z. Chen, X.-K. Liu, H. Wang, F. Gao
 Department of Physics, Chemistry, and Biology (IFM)
 Linköping University
 Linköping 58183, Sweden
 E-mail: xiaoke.liu@liu.se
 X. Liu
 Laboratory of Organic Electronics
 Department of Science and Technology
 Linköping University
 Norrköping 60174, Sweden

 The ORCID identification number(s) for the author(s) of this article can be found under <https://doi.org/10.1002/adom.202202528>.

© 2023 The Authors. Advanced Optical Materials published by Wiley-VCH GmbH. This is an open access article under the terms of the Creative Commons Attribution License, which permits use, distribution and reproduction in any medium, provided the original work is properly cited.

DOI: 10.1002/adom.202202528

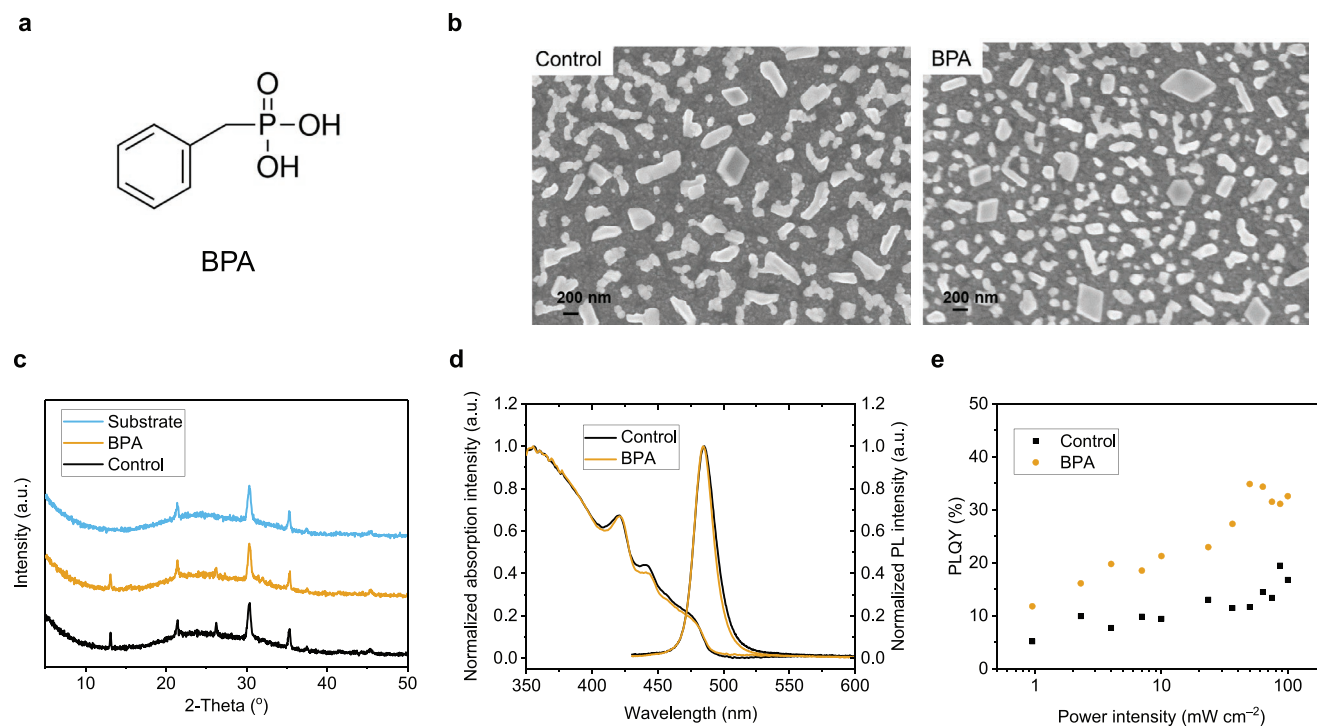


Figure 1. a) Chemical structure of BPA. b) SEM images, c) XRD patterns, d) normalized absorption and PL spectra, and e) PLQY-excitation intensity characteristics of the control and BPA-based perovskite films. For all these measurements, the perovskite films were fabricated on the substrate of ITO-coated glass/TFB/PVK/PVP.

boundaries and reduces the nonradiative recombination rate by suppressing electron–phonon interaction. The incorporation of BPA doubles the PLQY of the mixed Cl/Br perovskite film, consequently resulting in a doubled peak EQE of 6.3% in sky-blue PeLEDs. Moreover, we reveal severe thermal quenching in the blue perovskite films. Based on temperature-dependent PL measurements, we propose a two-step mechanism involving exciton dissociation and electron–phonon interaction to explain the thermal quenching behavior. Our results suggest that enhancing the radiative recombination rate and reducing the electron–phonon interaction-induced nonradiative recombination rate are crucial to achieving high-PLQY blue perovskite films at room temperature or above. This work provides an insightful understanding of the limiting factors of the PLQY of blue perovskite films and affords useful guidelines for the development of highly efficient blue PeLEDs.

2. Results and Discussion

2.1. PLQY Enhancement by BPA

The mixed Cl/Br perovskite film (denoted as control film) used in this study was prepared from precursors with an optimized molar ratio of 1.2: 0.25: 0.05: 1: 2.66: 1.44: 0.6 for Cs^+ : FA^+ : Rb^+ : Pb^{2+} : Br^- : Cl^- : BH^+ , where FA^+ is formamidinium, and BH is benzamidine. BH was used to stabilize the emission spectra of mixed Cl/Br perovskites as demonstrated in our previous study.^[27] The BPA-based perovskite film was fabricated following the procedures of the control film, except that 10 mol%

BPA (to the concentration of Pb^{2+}) was added in the precursor solution (see details in the Experimental Section).

We first investigate the physical properties of the control and BPA-based perovskite films. Figure 1b shows their scanning electron microscopy (SEM) images, which demonstrate similar morphologies with discontinuous perovskite grains. Figure 1c shows the X-ray diffraction (XRD) patterns of the two perovskite films with the substrate as a reference. Both perovskite films show XRD peaks at 13.1° and 26.2° , which are most likely from the (002) and (004) planes of $n = 2$ quasi-two-dimensional (2D) perovskite phase.^[9] Moreover, the XRD patterns of the two perovskite films exhibit similar diffraction intensities at the same 2-theta values. These observations indicate that BPA causes changes in neither the perovskite phase nor crystallinity. The absorption and PL spectra of the two perovskite films are shown in Figure 1d. Both show similar absorption spectra with excitonic peaks at 421 and 442 nm, which can be assigned to $n = 2$ and $n = 3$ quasi-2D perovskite phases, respectively.^[9] This agrees well with the XRD result, confirming the existence of quasi-2D perovskite phases in both perovskite films. Although the BPA-based film shows a slightly narrower PL spectrum than the control film, both PL spectra peak at 484 nm. Since the absorption band at around 475 nm shows an obvious feature of the three-dimensional (3D) perovskite phase,^[6,27] we speculate that the PL spectra are composed primarily of the emissions from the 3D phase. This is confirmed by the PLQY measurement at different excitation intensities. As shown in Figure 1e, the PLQYs of both the control and BPA-based films show obvious excitation power dependence, verifying that the PL emissions of both films originate from the free-carrier

recombination of the 3D perovskite phase rather than excitonic recombination of quasi-2D perovskite phases.^[1] Therefore, based on the results above, we can conclude that the two films are composed of mixed-dimensional perovskite phases, among which the 3D phase dominates the emission, although its occurrence is not indicated in the XRD patterns.

Figure 1e also clearly demonstrates that the PLQYs of the perovskite film are significantly enhanced by BPA. The PLQYs of the BPA-based film are 12% at the excitation power intensity of 1 mW cm⁻² and 32% at 100 mW cm⁻², in comparison to 5% and 17%, respectively, for the control film. To gain more insights into the doubled PLQYs, we study the PL decay characteristics of the two films. As shown in Figure S1 and Tables S1 and S2 (Supporting Information), the BPA-based perovskite film shows a slightly longer average PL lifetime of 2.50 ns than the control film (1.79 ns). Based on the average PL lifetimes and the PLQYs, we estimate the radiative and nonradiative recombination rate constants (Table S1 and S2, Supporting Information). Compared with the control film, the BPA-based perovskite film shows both reduced nonradiative recombination rate and enhanced radiative recombination rate, which are collectively responsible for the doubled PLQY. Note that BPA plays a negligible role in changing the crystallization process of the perovskite grains because of negligible changes in morphology and crystal structures.^[30] The reduced nonradiative recombination rate could be attributed to suppressed vibrations by BPA, as discussed later.

We investigate the origin of the enhanced radiative recombination rate, which could be explained as the change of surface electronic states caused by BPA. The increase of the radiative recombination rate is believed to be an intrinsic material property of perovskites, involving the change of electronic structure.^[31] As the electronic structures of perovskites are composed of orbitals of Pb and halide atoms,^[32] we use X-ray photoelectron spectroscopy (XPS) to investigate the binding energies of these species. As shown in Figure S2 (Supporting Information), the XPS peaks of Pb 4f, Cl 2p, and Br 3d core levels shift to lower binding energies after adding BPA, while those of the Cs 3d core levels keep unchanged, implying increasing electron density around the surficial lead halide species.^[33] This can be explained as the chemical interactions between Pb ions at the surface of perovskite grains and the electron-donating O=P/O-P groups of BPA molecules,^[34,35] which is confirmed by the transmission Fourier transform-infrared (FT-IR) measurement. Figure S3 (Supporting Information) shows the FT-IR spectra of pure BPA molecule and BPA + PbCl₂ blend, where after mixing with PbCl₂ obvious changes of BPA's $\nu(\text{P=O})$ and $\nu(\text{P-O})$ vibrations^[35,36] at around 1182, 1028, and 935 cm⁻¹ are observed. These results confirm the interactions between Pb and O=P/O-P, implying the formation of oxide-bonded perovskite (Pb-O) surface states which may fundamentally alter the electronic structure of the perovskite and consequently the radiative recombination rate.^[31,37]

2.2. Temperature-Dependent PL Characteristics

As demonstrated above, BPA is effective in promoting the PLQY of the perovskite emissive layer by both reducing the

nonradiative recombination rate and enhancing the radiative recombination rate. But the absolute PLQY of the BPA-based film is still not as high as unity, which inspires us to understand the underlying reason.

We first observed significant PL enhancement at low temperatures. As shown in Figure 2a,b, we measured the PL spectra of the control and BPA-based perovskite films at various temperatures ranging from 10 to 350 K. Besides the main emission peaks, emissions at shorter wavelengths occur with decreasing temperature. This phenomenon is more obvious for the control film (Figure S4, Supporting Information), in which the newly appeared emission peaks at around 430, 450, and 468 nm can be assigned to quasi-2D perovskites of $n = 2, 3$, and 4 phases, respectively. But the broad shorter-wavelength peaks of the BPA-based film originate from poly[(9,9-diocetylfluorenyl-2,7-diyl)-co-(4,4'-(N-(4-sec-butylphenyl)diphenylamine)] (TFB) of the substrate (Figure S4c, Supporting Information). Moreover, it is worth noting that the PL intensities of both films increase significantly with decreasing temperature (Figure 2a,b). Based on the integrated PL intensities at different temperatures and the PLQYs at room temperature,^[38] we reveal the relationship between PLQY and temperature for the control and BPA-based perovskite films (Figure 2c, Tables S1 and S2, Supporting Information). The PLQY of the BPA-based film reaches over 60% at 50 K, while the control film shows a maximum PLQY of 21% even at low temperatures.

Although the control and BPA-based perovskite films show largely different PLQYs, we find that they possess the same thermal-quenching mechanism. Figure 2d shows normalized integrated PL intensities of both films, which indicates that their PL intensities decay at similar rates with increasing temperature. This implies the same thermal-quenching mechanism both films undergo, even though they have large differences in PLQY at the same temperatures (Figure 2c). For a more quantitative analysis, we plotted the integrated PL intensity as a function of 1/temperature (1/T) (Figure S5, Supporting Information). For both films, the intensities are almost constant below 70 K, above which rapid PL quenching is observed. Generally, the temperature dependence of the integrated PL intensity, $I(T)$, can be described by

$$I(T) = \frac{I_0}{1 + Ae^{-E_a/k_B T}} \quad (2)$$

where I_0 is the PL intensity at 0 K, A is a constant, E_a is the activation energy of a metastable state leading to nonradiative decay, and k_B is the Boltzmann constant.^[39] Equation (2) can be written as

$$\ln\left(\frac{I_0}{I(T)} - 1\right) = -\frac{E_a}{k_B} \cdot \frac{1}{T} + \ln A \quad (3)$$

of which the slope of the curve $\ln\left(\frac{I_0}{I(T)} - 1\right)$ vs. $\frac{1}{T}$ gives the activation energy of the nonradiative decay channel.

Figure 2e,f shows the relationships between $\ln\left(\frac{I_0}{I(T)} - 1\right)$ and $\frac{1}{T}$ for the control and BPA-based perovskite films, respectively. Both films exhibit two slopes, indicating two nonradiative decay channels. For the best fit to the data (Figure 2e,f), we

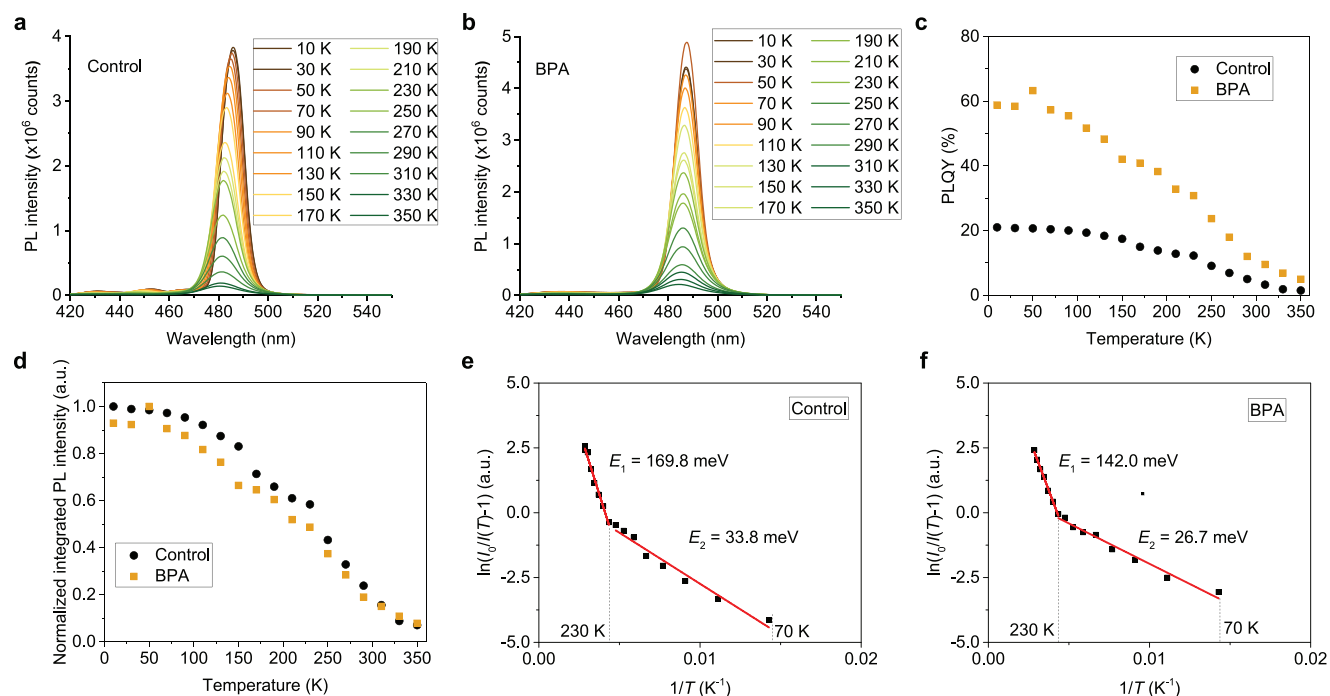


Figure 2. PL spectra of a) the control and b) BPA-based perovskite films at various temperatures. c) PLQYs and d) normalized integrated PL intensity (divided by max values) versus temperature. The relationships between $\ln\left(\frac{I_0}{I(T)} - 1\right)$ and $\frac{1}{T}$ and their fitting curves for e) the control and f) BPA-based perovskite films; the slopes give activation energies.

obtain the activation energies $E_1 = 169.8$ meV and $E_2 = 33.8$ meV for the control film and $E_1 = 142.0$ meV and $E_2 = 26.7$ meV for the BPA-based film. We hypothesize that the smaller energies (E_2) are attributed to the activation energies for exciton dissociation (that is, exciton binding energies)^[39] and the larger ones (E_1) to electron–phonon interaction.^[40,41]

We performed PL decay measurements at various temperatures to verify our hypothesis. As shown in Figure S6 (Supporting Information) and summarized in Tables S1 and S2 (Supporting Information), both films exhibit fast PL decays at 10 K, which gradually become slower as the temperature rises to 230 K. A reverse trend is observed when the temperature increases from 230 to 350 K. To gain more insights, we calculated the rate constants of total recombination (k_{total}), radiative recombination (k_r), and nonradiative recombination (k_{nr}) at different temperatures (Figure 3a,b, and Tables S1 and S2, Supporting Information). As shown in Figure 3a,b, above 70 K the k_r values of both films rapidly decrease with increasing temperature. This agrees well with the smaller activation energies (E_2), suggesting that the first thermal quenching channel can be assigned to the gradual transformation of the radiative recombination from fast excitonic to slow bimolecular types. Moreover, the k_{nr} values of both films decrease as temperature rises until around 230 K, which then increase rapidly. This observation is in line with the larger activation energies (E_1), indicating that the second thermal quenching channel is attributed to the increase in the nonradiative recombination rate.

We further confirm that the increase of nonradiative recombination above 230 K is related to the electron–longitudinal optical (LO) phonon coupling. As shown in Figure 3c,d, the PL spectra at 230 K are broader and less symmetric than

those at 10 and 70 K, suggesting the existence of electron–phonon interaction.^[42] We use temperature-dependent PL line widths to further elucidate the electron–phonon interaction. Figure 3e,f shows the full width at half maximum (FWHM) of the PL spectra as a function of temperature, which can be best modelled using Equation (4), by taking the inhomogeneous broadening and LO phonon scattering into consideration.

$$\text{FWHM} = \Gamma_0 + \frac{\Gamma_{\text{LO}}}{\exp\left(\frac{E_{\text{LO}}}{k_{\text{B}}T}\right) - 1} \quad (4)$$

where Γ_0 is the inhomogeneous linewidth, which is determined by structural disorder, Γ_{LO} is electron–LO–phonon coupling strength and E_{LO} is phonon energy. The fitting parameters are summarized in Table S3 (Supporting Information). To gain more insights into the intensity of the electron–phonon interaction, we compared the deformation potential (D)—the shift in energy band per unit strain—of both films by using Equation (5).^[41] The result suggests that the deformation potential in the control film is 2.7 times higher than that in the BPA-based perovskite film, implying that BPA can suppress electron–phonon interaction.^[41] This finding corroborates the observed slower k_{nr} and higher PLQY for the BPA-based film in comparison to those of the control film.

$$D \propto (\Gamma_{\text{LO}} E_{\text{LO}})^{\frac{1}{2}} \quad (5)$$

Based on the results above, we now can elucidate the thermal quenching mechanism of the blue perovskite films. Below 70 K, excitons are responsible for the radiative decay, and the PL

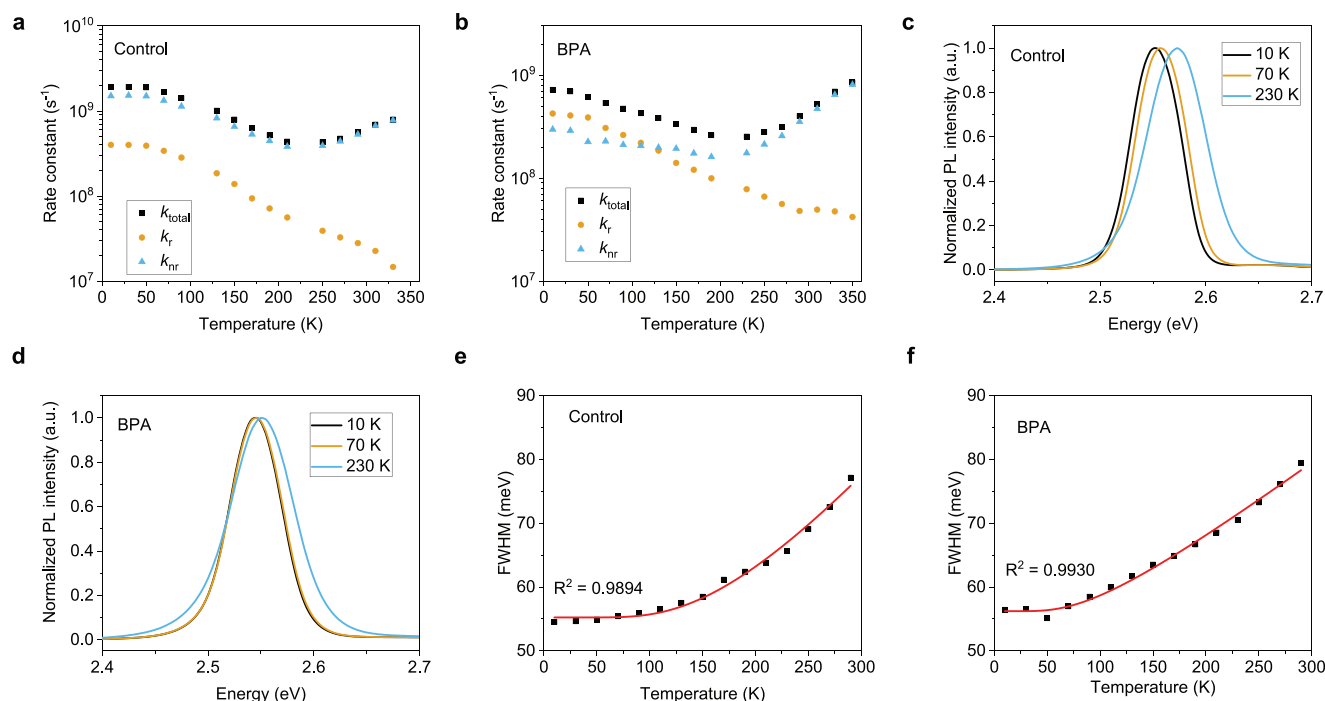


Figure 3. The rate constants of k_{total} , k_r , and k_{nr} at different temperatures for a) the control and b) BPA-based perovskite films. Normalized PL spectra at 10, 70, and 230 K for c) the control and d) BPA-based films. PL linewidth as a function of temperature and their fitting curves for e) the control and f) BPA-based perovskite films.

intensity is negligibly quenched with increasing temperature. At 70–230 K, the excitons start to overcome the exciton binding energy and dissociate into free charge carriers, resulting in the transformation from fast excitonic radiative recombination to slow bimolecular radiative recombination. As the temperature continues to rise above 230 K, electron–phonon interaction dominates, causing a rapid increase in the nonradiative recombination rate and a significant decrease in PLQY.

2.3. Enhanced Efficiency in Sky-Blue PeLEDs

We fabricated blue PeLEDs based on the control and BPA-based perovskite films. A device structure (Figure 4a) of indium tin oxide (ITO)/TFB/poly(9-vinylcarbazole) (PVK)/poly(4-vinylpyridine) (PVP)/perovskite/1,3,5-tris(1-phenyl-1H-benzimidazol-2-yl)benzene (TPBi, 35 nm)/lithium fluoride (1 nm)/aluminum (100 nm) is employed. The TFB/PVK bilayer is adopted to facilitate hole injection owing to a cascade energy level alignment,^[43] while the PVP layer is used to improve the wettability of the perovskite precursor solution on the PVK surface.^[6]

Current density–voltage–luminance and EQE–current density characteristics of the PeLEDs are shown in Figure 4b,c, respectively. The BPA-based device shows a turn-on voltage of 2.9 V (measured at 1 cd cm^{−2}), which is negligibly lower than that of the control device. Nevertheless, it is observed that BPA suppresses leakage current and significantly promotes the luminance from 447 to 1926 cd cm^{−2}. Meanwhile, the EQE is enhanced by BPA from 3.0% to 6.3% (Figure 4c and Table S4, Supporting Information). The trend in EQE is in line with the PLQY result, indicating that the PLQY enhancement of the perovskite emissive layer is responsible for the doubled EQE.

Figure S7 (Supporting Information) shows the histograms of the EQEs of the control and BPA-based PeLEDs, demonstrating an average EQE of 1.5% and 4.4%, respectively.

The spectral stability of the mixed halide PeLEDs is examined. As shown in Figure 4d,e, both control and BPA-based devices show stable electroluminescence (EL) spectra at different driving voltages, albeit slightly broadening at high driving voltages. The control device has an EL peak at 486 nm with FWHM of 18–22 nm and CIE chromaticity coordinates of (0.08, 0.22). The values are 489 nm, 17–21 nm and (0.07, 0.29) for the BPA-based device (Table S4, Supporting Information). We tested the stability of the control and BPA-based PeLEDs (Figure S8, Supporting Information). The T_{50} (the time taken for the luminance to drop to half of its initial value) measured at an initial luminance of 60 cd cm^{−2} is about 20 s for the control device and 200 s for the BPA-based device. Note that the device stability of blue PeLEDs represents another critical challenge as the lifetimes of the reported most stable blue PeLEDs are only several hours.^[13] Despite the unsatisfactory lifetime, our PeLED shows no spectral shift during operation (Figure 4f). The excellent spectral stability of these mixed halide PeLEDs can be attributed to the unique role of BHCl as demonstrated in our previous report.^[27]

3. Conclusions

In summary, we have demonstrated considerably enhanced PLQY in the mixed Cl/Br perovskite films by incorporating a molecule, BPA, which promotes the radiative recombination rate and reduces the nonradiative recombination rate. The former can be assigned to the formation of oxide-bonded

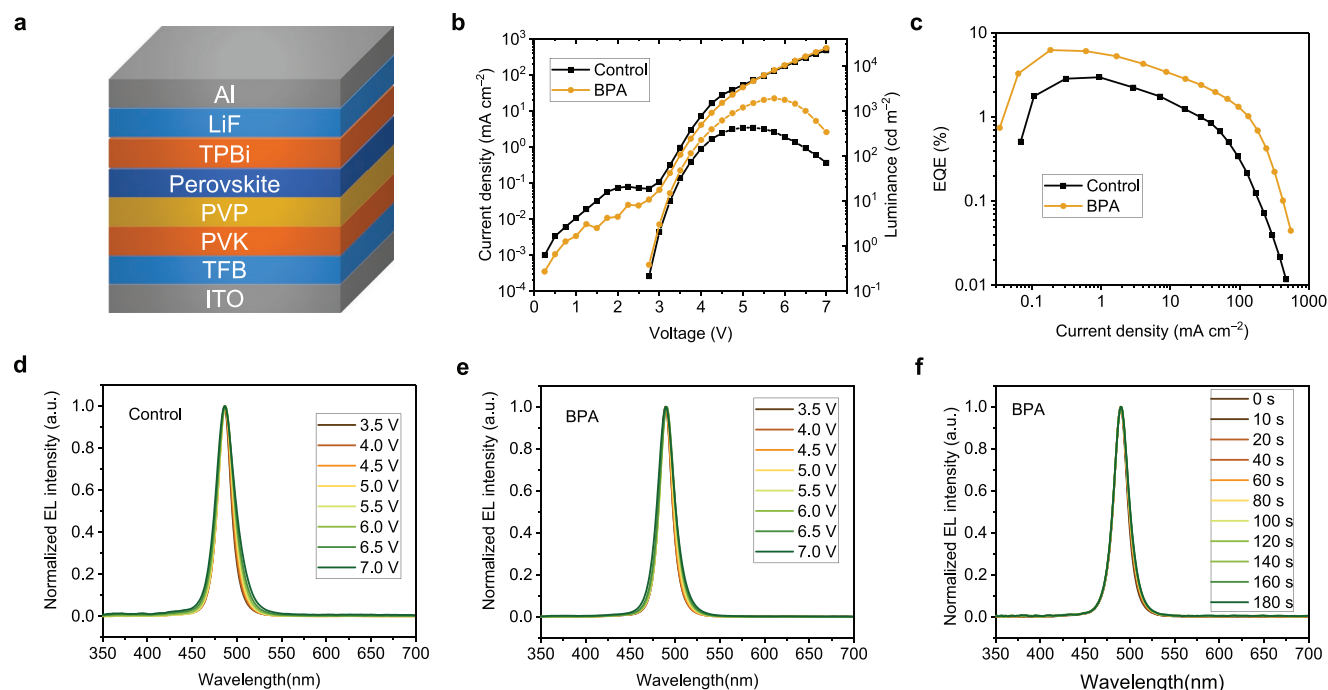


Figure 4. a) Schematic of device architecture. b) Current density–voltage–luminance and c) EQE-current density curves for the control and BPA-based PeLEDs. EL spectra of d) the control device and e) the BPA-based device at different driving voltages. f) EL spectra of the BPA-based device, recorded during continuous operation.

perovskite surface at grain boundaries, while the latter results from suppressed electron–phonon interaction. Owing to the enhanced PLQY, BPA doubles the EQE to 6.3% in sky-blue PeLEDs. Moreover, we have observed significant thermal quenching in the mixed Cl/Br blue perovskite films, which appears to be a significant factor limiting the efficiency of blue PeLEDs at room temperature or above. We have proposed a two-step mechanism consisting of exciton dissociation and electron–phonon interaction to elucidate the thermal quenching phenomenon. Our results highlight that it is important to enhance the radiative recombination rate and reduce the intrinsic nonradiative recombination rate for achieving high-PLQY blue perovskite films at room temperature or above. This work provides new understandings of photoluminescence enhancement and affords useful guidelines for designing highly efficient blue perovskite materials.

4. Experimental Section

Materials: Cesium bromide (CsBr, 99.9%) was purchased from Alfa Aesar and formamidinium bromide (FABr, >99.99%) from GreatCell Solar Limited. Rubidium bromide (RbBr, 99.6%), lead bromide (PbBr₂, 99.999%), lead chloride (PbCl₂, 99.999%), benzamidine hydrochloride (BHCl, 99%), benzylphosphonic acid (BPA, 97%), poly(9-vinylcarbazole) (PVK, average $M_w \approx 1\,100\,000$), poly(vinyl alcohol) (PVA, $M_w \approx 89\,000$ – $98\,000$, 99+% hydrolyzed), poly(4-vinylpyridine) (PVP, average $M_w \approx 60\,000$), lithium fluoride (LiF, precipitated, 99.995%), and dimethyl sulfoxide (DMSO, anhydrous, >99.9%) were purchased from Sigma-Aldrich. 1,3,5-Tris(1-phenyl-1H-benzimidazol-2-yl) benzene (TPBi, sublimed, >99.8%) and poly[(9,9-dioctylfluorenyl-2,7-diyl)-co-(4,4'-(N-(4-sec-butylphenyl)diphenylamine))] (TFB, $M_w > 30\,000$) were purchased from Lumtec.

Preparation of Perovskite Precursor Solutions: CsBr, FABr, RbBr, PbBr₂, PbCl₂, BHCl, and BPA were dissolved in DMSO separately to obtain solutions with concentrations of 0.2, 0.5, 0.1, 0.4, 0.4, 1.0, 0.1 M, respectively. PVA was dissolved in DMSO with a concentration of 20 mg mL⁻¹. The perovskite precursor solutions were prepared by mixing those solutions. For the control solution, a molar ratio of 1.2:0.25:0.05:0.58:0.42:0.6 for CsBr: FABr: RbBr: PbBr₂: PbCl₂: BHCl and a concentration of 3 mg mL⁻¹ for PVA were used. For the BPA-based perovskite solution, 10 mol% BPA (to the concentration of Pb²⁺) was added to the control solution. The concentration of Pb²⁺ for all the perovskite precursor solutions was kept at 0.07 M.

Preparation of Perovskite Films: ITO-coated glass substrates were washed using detergent and then ultrasonically cleaned in deionized water for 15 min. They were dried by high-speed nitrogen flow before being placed in an ultraviolet–ozone cleaner for 10 min. The clean ITO substrates were then transported into a nitrogen-filled glovebox for film fabrication. TFB (6 mg mL⁻¹ in chlorobenzene) was spin-coated on the ITO substrates at 6000 rpm for 30 s, followed by thermal annealing at 130 °C for 10 min. PVK (4 mg mL⁻¹ in chlorobenzene) was sequentially deposited at 2000 rpm for 30 s and then annealed at 130 °C for 10 min. PVP (2 mg mL⁻¹ in isopropanol) was prepared at 3000 rpm for 30 s and annealed at 100 °C for 5 min. The perovskite films were fabricated from their precursor solutions at 4000 rpm for 30 s, followed by dimethylformamide (DMF) vapor-assisted annealing^[44] at 80 °C for 20 min.

Preparation and Characterization of PeLEDs: To fabricate the PeLEDs, the perovskite films were transported into a vacuum chamber. Under vacuum of $<4 \times 10^{-6}$ mbar, TPBi (35 nm), LiF (1 nm), and Al (100 nm) were sequentially deposited at the rates of 1.5, 0.2, and 5.0 Å s⁻¹, respectively. The active emitting area of the PeLEDs was 0.0725 cm², determined by the overlap of the patterns of ITO and the Al electrodes. The PeLEDs were characterized in a nitrogen-filled glovebox at room temperature. The current density and voltage of the devices were recorded by a Keithley 2400 source meter. The forward-viewing spectral radiant flux was measured by a homemade setup with an integrating sphere and a QE65 Pro spectrometer. The stability of the PeLEDs was measured using the same setup.

Film Characterizations: The SEM images were obtained by a Philips XL 30 FEG scanning electron microscope. The XRD measurements were performed using an X-ray diffractometer (PANalytical X'Pert Pro) equipped with a Cu K α source ($\lambda = 1.5406 \text{ \AA}$). The UV–vis absorption spectra were recorded with a PerkinElmer model Lambda 900 spectrometer. The steady-state PL spectra were measured by a Newton Andor spectrometer (Shamrock sr-303i-B, with a Newton EMCCD Si array detector) with a 405 nm continuous-wave laser. For temperature-dependent measurements, the temperature was initially decreased from room temperature to 10 K using a helium compressor, and gradually heated up to 350 K; the measurements were made during the heat-up process. The PLQY results were obtained by an integrated system of a 405 nm laser, optical fiber, spectrometer, and an integrating sphere. The PL decay measurements were conducted using a homemade setup with an ID100 visible single-photon detector, a time tagging device (quTAG), and a 405 nm pulsed laser (Edinburgh Instruments EPL-405). The XPS measurements were performed in an ultrahigh vacuum ($\approx 1 \times 10^{-10}$ mbar) using a Scienta ESCA 200 spectrometer coupled with a monochromatic Al (K α) X-ray source, which provides photons of 1486.6 eV. All spectra were measured at a photoelectron take-off angle of 0° (normal emission). The XPS experimental condition was set so that the FWHM of the clean Au 4f7/2 line (at the binding energy of 84.00 eV) was 0.65 eV. The FT-IR spectra were recorded from a PIKE MIRacle ATR accessory with a diamond prism in a Vertex 70 Spectrometer (Bruker) at room temperature.

Supporting Information

Supporting Information is available from the Wiley Online Library or from the author.

Acknowledgements

This work was financially supported by the Swedish Energy Agency Energimyndigheten (No. 48758-1). Z.C. thanks the project funded by China Postdoctoral Science Foundation (2020M673055). L.H. thanks the NSFC Project (61774077) and the Research and Development Program in Key Areas of Guangdong Province (2019B1515120073, 2019B090921002, 2019B010132004) for financial support. Z.C. is a Marie Skłodowska-Curie Fellow (No. 895679). The authors thank B. Yang for the assistance in the PL decay and FT-IR measurements.

Conflict of Interest

The authors declare no conflict of interest.

Data Availability Statement

The data that support the findings of this study are available from the corresponding author upon reasonable request.

Keywords

blue perovskites, light-emitting diodes, mixed halides, PeLEDs, photoluminescence

Received: October 25, 2022

Revised: December 3, 2022

Published online:

- [1] X.-K. Liu, W. Xu, S. Bai, Y. Jin, J. Wang, R. H. Friend, F. Gao, *Nat. Mater.* **2021**, 20, 10.
- [2] J. S. Kim, J.-M. Heo, G.-S. Park, S.-J. Woo, C. Cho, H. J. Yun, D.-H. Kim, J. Park, S.-C. Lee, S.-H. Park, E. Yoon, N. C. Greenham, T.-W. Lee, *Nature* **2022**, 611, 688.
- [3] Z. Liu, W. Qiu, X. Peng, G. Sun, X. Liu, D. Liu, Z. Li, F. He, C. Shen, Q. Gu, F. Ma, H.-L. Yip, L. Hou, Z. Qi, S.-J. Su, *Adv. Mater.* **2021**, 33, 2103268.
- [4] J. Jiang, Z. Chu, Z. Yin, J. Li, Y. Yang, J. Chen, J. Wu, J. You, X. Zhang, *Adv. Mater.* **2022**, 34, 2204460.
- [5] B. Guo, R. Lai, S. Jiang, L. Zhou, Z. Ren, Y. Lian, P. Li, X. Cao, S. Xing, Y. Wang, W. Li, C. Zou, M. Chen, Z. Hong, C. Li, B. Zhao, D. Di, *Nat. Photonics* **2022**, 16, 637.
- [6] M. Karlsson, Z. Yi, S. Reichert, X. Luo, W. Lin, Z. Zhang, C. Bao, R. Zhang, S. Bai, G. Zheng, P. Teng, L. Duan, Y. Lu, K. Zheng, T. Pullerits, C. Deibel, W. Xu, R. Friend, F. Gao, *Nat. Commun.* **2021**, 12, 361.
- [7] Y. Liu, J. Cui, K. Du, H. Tian, Z. He, Q. Zhou, Z. Yang, Y. Deng, D. Chen, X. Zuo, Y. Ren, L. Wang, H. Zhu, B. Zhao, D. Di, J. Wang, R. H. Friend, Y. Jin, *Nat. Photonics* **2019**, 13, 760.
- [8] Z. Chu, Y. Zhao, F. Ma, C.-X. Zhang, H. Deng, F. Gao, Q. Ye, J. Meng, Z. Yin, X. Zhang, J. You, *Nat. Commun.* **2020**, 11, 4165.
- [9] Q. Wang, X. Wang, Z. Yang, N. Zhou, Y. Deng, J. Zhao, X. Xiao, P. Rudd, A. Moran, Y. Yan, J. Huang, *Nat. Commun.* **2019**, 10, 5633.
- [10] Y. Dong, Y.-K. Wang, F. Yuan, A. Johnston, Y. Liu, D. Ma, M.-J. Choi, B. Chen, M. Chekini, S.-W. Baek, L. K. Sagar, J. Fan, Y. Hou, M. Wu, S. Lee, B. Sun, S. Hoogland, R. Quintero-Bermudez, H. Ebe, P. Todorovic, F. Dinic, P. Li, H. T. Kung, M. I. Saidaminov, E. Kumacheva, E. Spiecker, L.-S. Liao, O. Voznyy, Z.-H. Lu, E. H. Sargent, *Nat. Nanotechnol.* **2020**, 15, 668.
- [11] Z. Zhu, Y. Wu, Y. Shen, J. Tan, D. Shen, M.-F. Lo, M. Li, Y. Yuan, J.-X. Tang, W. Zhang, S.-W. Tsang, Z. Guan, C.-S. Lee, *Chem. Mater.* **2021**, 33, 4154.
- [12] Z. Ren, K. Wang, X. W. Sun, W. C. H. Choy, *Adv. Funct. Mater.* **2021**, 31, 2100516.
- [13] A. Mishra, M. Alahbakhshi, R. Haroldson, Q. Gu, A. A. Zakhidov, J. D. Slinker, *Adv. Funct. Mater.* **2021**, 31, 2102006.
- [14] Y. Shen, Y.-Q. Li, K. Zhang, L.-J. Zhang, F.-M. Xie, L. Chen, X.-Y. Cai, Y. Lu, H. Ren, X. Gao, H. Xie, H. Mao, S. Kera, J.-X. Tang, *Adv. Funct. Mater.* **2022**, 32, 2206574.
- [15] Y. Tong, X. Bi, S. Xu, H. Min, L. Cheng, Z. Kuang, L. Yuan, F. Zhou, Y. Chu, L. Xu, L. Zhu, N. Zhao, N. Wang, W. Huang, J. Wang, *Adv. Mater.* **2022**, 34, 2207111.
- [16] S. D. Stranks, R. L. Z. Hoyer, D. Di, R. H. Friend, F. Deschler, *Adv. Mater.* **2019**, 31, 1803336.
- [17] J. C. Scott, G. G. Malliaras, in *Semiconducting Polymer*, (Eds: G. Hadzioannou, P.F. vanHutten), Wiley-VCH, Weinheim, Germany **1999**, Ch. 13.
- [18] N. K. Kumawat, A. Dey, A. Kumar, S. P. Gopinathan, K. L. Narasimhan, D. Kabra, *ACS Appl. Mater. Interfaces* **2015**, 7, 13119.
- [19] A. Sadhanala, S. Ahmad, B. Zhao, N. Giesbrecht, P. M. Pearce, F. Deschler, R. L. Z. Hoyer, K. C. Gödel, T. Bein, P. Docampo, S. E. Dutton, M. F. L. De Volder, R. H. Friend, *Nano Lett.* **2015**, 15, 6095.
- [20] Y. R. Park, H. H. Kim, S. Eom, W. K. Choi, H. Choi, B. R. Lee, Y. Kang, *J. Mater. Chem. C* **2021**, 9, 3608.
- [21] Y. J. Yoon, K. T. Lee, T. K. Lee, S. H. Kim, Y. S. Shin, B. Walker, S. Y. Park, J. Heo, J. Lee, S. K. Kwak, G.-H. Kim, J. Y. Kim, *Joule* **2018**, 2, 2105.
- [22] Q. A. Akkerman, V. D'Innocenzo, S. Accornero, A. Scarpellini, A. Petrozza, M. Prato, L. Manna, *J. Am. Chem. Soc.* **2015**, 137, 10276.
- [23] H. Wang, Y. Xu, J. Wu, L. Chen, Q. Yang, B. Zhang, Z. Xie, *J. Phys. Chem. Lett.* **2020**, 11, 1411.

- [24] Z. Ren, L. Li, J. Yu, R. Ma, X. Xiao, R. Chen, K. Wang, X. W. Sun, W.-J. Yin, W. C. H. Choy, *ACS Energy Lett.* **2020**, *5*, 2569.
- [25] S. Hou, M. K. Gangishetty, Q. Quan, D. N. Congreve, *Joule* **2018**, *2*, 2421.
- [26] X. Zheng, S. Yuan, J. Liu, J. Yin, F. Yuan, W.-S. Shen, K. Yao, M. Wei, C. Zhou, K. Song, B.-B. Zhang, Y. Lin, M. N. Hedhili, N. Wehbe, Y. Han, H.-T. Sun, Z.-H. Lu, T. D. Anthopoulos, O. F. Mohammed, E. H. Sargent, L.-S. Liao, O. M. Bakr, *ACS Energy Lett.* **2020**, *5*, 793.
- [27] H. Yu, H. Wang, T. Zhang, C. Yi, G. Zheng, C. Yin, M. Karlsson, J. Qin, J. Wang, X.-K. Liu, F. Gao, *J. Phys. Chem. Lett.* **2021**, *12*, 6041.
- [28] W. Li, H. Zhang, C. Yu, T. Li, X. Zhang, C. Xiong, T. Wang, *ACS Appl. Electron. Mater.* **2021**, *3*, 4912.
- [29] S. Yuan, L.-S. Cui, L. Dai, Y. Liu, Q.-W. Liu, Y.-Q. Sun, F. Auras, M. Anaya, X. Zheng, E. Ruggeri, Y.-J. Yu, Y.-K. Qu, M. Abdi-Jalebi, O. M. Bakr, Z.-K. Wang, S. D. Stranks, N. C. Greenham, L.-S. Liao, R. H. Friend, *Adv. Mater.* **2021**, *33*, 2103640.
- [30] H. Wang, F. U. Kosasih, H. Yu, G. Zheng, J. Zhang, G. Pozina, Y. Liu, C. Bao, Z. Hu, X. Liu, L. Kobera, S. Abbrent, J. Brus, Y. Jin, M. Fahlman, R. H. Friend, C. Ducati, X.-K. Liu, F. Gao, *Nat. Commun.* **2020**, *11*, 891.
- [31] S. Feldmann, M. K. Gangishetty, I. Bravić, T. Neumann, B. Peng, T. Winkler, R. H. Friend, B. Monserrat, D. N. Congreve, F. Deschler, *J. Am. Chem. Soc.* **2021**, *143*, 8647.
- [32] M. Wuttig, C.-F. Schön, M. Schumacher, J. Robertson, P. Golub, E. Bousquet, C. Gatti, J.-Y. Raty, *Adv. Funct. Mater.* **2022**, *32*, 2110166.
- [33] J. He, J. Liu, Y. Hou, Y. Wang, S. Yang, H. G. Yang, *Nat. Commun.* **2020**, *11*, 4237.
- [34] M. Li, Y. Zhao, X. Qin, Q. Ma, J. Lu, K. Lin, P. Xu, Y. Li, W. Feng, W.-H. Zhang, Z. Wei, *Nano Lett.* **2022**, *22*, 2490.
- [35] T. Schulmeyer, S. A. Paniagua, P. A. Veneman, S. C. Jones, P. J. Hotchkiss, A. Mudalige, J. E. Pemberton, S. R. Marder, N. R. Armstrong, *J. Mater. Chem.* **2007**, *17*, 4563.
- [36] S. A. Paniagua, P. J. Hotchkiss, S. C. Jones, S. R. Marder, A. Mudalige, F. S. Marrikar, J. E. Pemberton, N. R. Armstrong, *J. Phys. Chem. C* **2008**, *112*, 7809.
- [37] H. Dong, C. Zhang, W. Nie, S. Duan, C. N. Saggau, M. Tang, M. Zhu, Y. S. Zhao, L. Ma, O. G. Schmidt, *Angew. Chem., Int. Ed.* **2022**, *61*, e202115875.
- [38] S. D. Stranks, V. M. Burlakov, T. Leijtens, J. M. Ball, A. Goriely, H. J. Snaith, *Phys. Rev. Appl.* **2014**, *2*, 034007.
- [39] T. J. Savenije, C. S. Ponseca, L. Kunneman, M. Abdellah, K. Zheng, Y. Tian, Q. Zhu, S. E. Canton, I. G. Scherblykin, T. Pullerits, A. Yartsev, V. Sundström, *J. Phys. Chem. Lett.* **2014**, *5*, 2189.
- [40] H. C. Woo, J. W. Choi, J. Shin, S.-H. Chin, M. H. Ann, C.-L. Lee, *J. Phys. Chem. Lett.* **2018**, *9*, 4066.
- [41] X. Gong, O. Voznyy, A. Jain, W. Liu, R. Sabatini, Z. Piontkowski, G. Walters, G. Bappi, S. Nokhrin, O. Bushuyev, M. Yuan, R. Comin, D. McCamant, S. O. Kelley, E. H. Sargent, *Nat. Mater.* **2018**, *17*, 550.
- [42] S. Peng, Q. Wei, B. Wang, Z. Zhang, H. Yang, G. Pang, K. Wang, G. Xing, X. W. Sun, Z. Tang, *Angew. Chem., Int. Ed.* **2020**, *59*, 22156.
- [43] J. Qing, S. Ramesh, Q. Xu, X.-K. Liu, H. Wang, Z. Yuan, Z. Chen, L. Hou, T. C. Sum, F. Gao, *Adv. Mater.* **2021**, *33*, 2104381.
- [44] J. Qing, X.-K. Liu, M. Li, F. Liu, Z. Yuan, E. Tiukalova, Z. Yan, M. Duchamp, S. Chen, Y. Wang, S. Bai, J.-M. Liu, H. J. Snaith, C.-S. Lee, T. C. Sum, F. Gao, *Adv. Energy Mater.* **2018**, *8*, 1800185.